but the resolution of ~2″ was not sufficient to determine whether the $C^{18}O$ emission was confined to a circumbinary structure, the remnant cloud core, or a combination of the two.
36. B. Reipurth, *Astron. J.* **120**, 3177 (2000).
37. E. L. N. Jensen, R. D. Mathieu, G. A. Fuller, *Astrophys. J. Lett.* **429**, L29 (1994).
38. S. H. Lubow, P. Artymowicz, in *Protostars and Planets IV*, V. Mannings, A. Boss, S. Russell, Eds. (Univ. of Arizona Press, Tucson, 2000), pp. 731–755.
39. A. I. Sargent, in *Disks and Outflows Around Young Stars*, S. V. W. Beckwith, A. Natta, J. Staude, Eds. (Springer-Verlag, Berlin, 1995), pp. 1–17.
40. G. Laughlin, P. Bodenheimer, *Astrophys. J.* **436**, 335 (1994).
41. H. W. Yorke, P. Bodenheimer, G. Laughlin, *Astrophys. J.* **443**, 199 (1995).
42. J. M. Stone, C. F. Gammie, S. A. Balbus, J. F. Hawley, in *Protostars and Planets IV*, V. Mannings, A. Boss, S. Russell, Eds. (Univ. of Arizona Press, Tucson, 2000), pp. 589–611.
43. R. Cesaroni *et al.*, *Astron. Astrophys.* **345**, 949 (1999).
44. L. Moscadelli, R. Cesaroni, M. J. Rioja, *Astron. Astrophys.* **360**, 663 (2000).
45. L. F. Rodríguez *et al.*, *Astrophys. J.* **430**, L65 (1994).
46. G. Narayanan, C. K. Walker, *Astrophys. J.* **466**, 844 (1996).
47. J. Martí, L. F. Rodríguez, J. M. Torrelles, *Astron. Astrophys.* **345**, L5 (1999).
48. J. Eislöffel, R. Mundt, T. P. Ray, L. F. Rodríguez, in *Protostars and Planets IV*, V. Mannings, A. Boss, S. Russell, Eds. (Univ. of Arizona Press, Tucson, 2000), pp. 815–840.
49. R. Ouyed, R. E. Pudritz, *Mon. Not. R. Astron. Soc.* **309**, 233 (1999).
50. R. J. Sault, P. J. Teuben, M. C. H. Wright, in *Astronomical Data Analysis Software and Systems IV*, vol. 77 of *PASP Conference Series*, R. A. Shaw, H. E. Payne, J. J. E. Hayes, Eds. (Astronomical Society of the Pacific, San Francisco, 1995), pp. 433–437.
51. The National Radio Astronomy Observatory (NRAO) is a facility of the National Science Foundation operated under cooperative agreement by Associated Universities, Inc. (AUI). We would like to thank G. Chavez and R. Hayward for building and optimizing the 7-mm receivers at the VLA. Without their efforts, observations of this caliber would not have been possible. We thank the entire team of NRAO staff working on the VLA-PT link project, in particular, R. Beresford and K. Sowinski for developing and supporting the VLA-PT link. Finally, we are grateful to the NSF and AUI for funding the PT link project and to Western New Mexico Telephone Company for the use of the fiber.

1 February 2001; accepted 11 April 2001

Spatially Resolved Spin-Injection Probability for Gallium Arsenide

V. P. LaBella,[1]* D. W. Bullock,[1] Z. Ding,[1] C. Emery,[1] A. Venkatesan,[1] W. F. Oliver,[1] G. J. Salamo,[1] P. M. Thibado,[1] M. Mortazavi[2]

We report a large spin-polarized current injection from a ferromagnetic metal into a nonferromagnetic semiconductor, at a temperature of 100 Kelvin. The modification of the spin-injection process by a nanoscale step edge was observed. On flat gallium arsenide [GaAs(110)] terraces, the injection efficiency was 92%, whereas in a 10-nanometer-wide region around a [$\bar{1}$11]-oriented step the injection efficiency is reduced by a factor of 6. Alternatively, the spin-relaxation lifetime was reduced by a factor of 12. This reduction is associated with the metallic nature of the step edge. This study advances the realization of using both the charge and spin of the electron in future semiconductor devices.

The ability to exploit the spin of the electron in semiconductor devices has the potential to revolutionize the electronics industry (*1*–*3*). The realization of "spintronic" devices is growing nearer as sources for spin-polarized electrons have become available in both ferromagnetic metals and ferromagnetic semiconductors (*4*, *5*). In addition, polarized electrons can move up to 100 μm in gallium arsenide (GaAs) without losing their polarization, so that coherent transport through the active region of a device structure is feasible (*6*). However, one of the most difficult challenges in creating "spintronic" devices is the ability to transfer the polarized electrons from a ferromagnetic material into a nonferromagnetic semiconductor without substantially degrading the polarization. For example, ferromagnetic metal contacts give spin-injection efficiencies of only a few percent at 4 K (*7*, *8*). Injection efficiencies using ferromagnetic semiconductors as contacts are as high as 90%; however, this is also only at 4 K (*9*–*11*). From the success of the all-semiconductor approach, it is thought that an epitaxial lattice-matched system is required for efficient spin injection. However, recent findings have demonstrated high injection efficiencies even with large lattice mismatches (*11*). These results have sparked renewed interest in determining the origin of spin-flip scattering mechanisms on a nanometer-length scale.

Tunneling-induced luminescence microscopy (TILM) makes it possible to correlate nanoscale features with their optical properties by injecting electrons and measuring the recombination luminescence (*12*–*14*). This technique cannot correlate the spin of the electron to any properties of the sample. However, with a spin-polarized scanning tunneling spectroscopy (STS) technique that incorporates a ferromagnetic metal tip, a net polarization in the recombination luminescence can be measured and related to the polarization state of the electrons at the time of recombination (*15*, *16*). This type of measurement has shown that vacuum tunneling preserves the spin-polarization properties of the electrons. The addition of the ability to correlate a surface feature seen in the topography of a scanning tunneling microscopy (STM) image with the degree of spinflip scattering is needed to better understand what affects the spin-injection process. For example, simultaneous imaging and spin-injection probability mapping of a surface would allow one to uncover what features and what mechanisms disrupt the spin-injection process.

We demonstrate that a large spin-polarized (~92%) current can be injected into GaAs at high temperatures (100 K). In addition, [$\bar{1}$11]-oriented steps are found to substantially decrease the injection efficiency (by a factor of 6). This observation is correlated to the density of midgap states.

A 100% spin-polarized STM tip was used as the electron source to locally inject polarized electrons into a p-type GaAs(110) surface while simultaneously measuring the polarization of the recombination luminescence. This spin-polarized TILM is similar to TILM, with the additional features that the injected electrons are spin polarized and the polarization state of the recombination luminescence is measured (*12*–*14*).

A polarized electron current was generated from a ferromagnetic single-crystal Ni<110> wire. Along the <110> direction in Ni, the density of spin-down states at the Fermi level is nonzero whereas the density of spin-up states is zero (*17*). Therefore, only the spin-down electrons contribute to conduction. The direction of the magnetization of the tips was determined to lie along the long axis of the wire as measured by a superconducting quantum interference device magnetometer. In addition, the wire was determined to have a remnant field of 0.3 Oe and a coercive field of 30 Oe; for additional experimental details, see (*18*).

Electrons injected into the empty conduction band states of GaAs eventually recombine across the 1.49-eV (100 K) band gap, emitting light, which is collected using a biconvex lens having an f-number of 1.0. The lens is mounted in situ and positioned 12.7

[1]Department of Physics, University of Arkansas, Fayetteville, AR 72701, USA. [2]Department of Physics, University of Arkansas, Pine Bluff, AR 71601, USA.

*To whom correspondence should be addressed. E-mail: vlabella@uark.edu

mm from the Ni tip (the focal length of the lens). The position of the lens was optimized with an external micrometer-controlled wobble stick with five degrees of freedom (three translational and two rotational). After passing through the lens, the light passes through an ultra-high-vacuum (UHV) viewport to polarization-sensitive optics. The optics contain a λ/4 retarder that is tuned to the band gap of GaAs (i.e., 832 nm), which is fastened in a two-position mount. The first position (A) converts right circularly polarized (RCP) light into a horizontal linear component and converts left circularly polarized (LCP) light into a vertical linear component, while the second position (B) does the opposite. Finally, a linear polarizer (with an extinction ratio >1000:1) passes through only the horizontal component to a high-sensitivity, cooled photomultiplier tube (PMT) configured to convert ~4000 photons/s to 1 nA of current. In this way, by manually switching between position A and B, the intensities of the RCP and LCP light are measured. The axis of the optics and thus the propagating direction of the measured photons is oriented ~60° from the tip and ~80° from the [$\bar{1}$10] direction of the GaAs crystal to minimize the effect of spontaneous electron polarization in GaAs (*19*).

The current from the PMT is measured using two complementary methods: a digital storage oscilloscope and the STM computer. The digital storage oscilloscope essentially allows continuous sampling of the PMT signal, whereas the STM computer is configured to read the PMT signal simultaneously with the topography and tunneling current pixel by pixel. As a result, the STM measurement provides a detailed topographical map and a tunneling-current map, and the corresponding intensities of the light at the local position of the STM tip. Typically, multiple sets of images of one area are acquired with the retarder in positions A and B to obtain pixel-by-pixel RCP and LCP light intensities, respectively, as well as for signal averaging purposes.

The intensities of the RCP (I_{RCP}) and LCP (I_{LCP}) tunneling-induced luminescence emitted from the GaAs sample were measured with the oscilloscope and were recorded while the Ni<110>STM tip was tunneling over a flat terrace region with a sample bias of 3.5 V and a tunneling current of 12 nA and with the tip's magnetization vector pointing both toward and away from the surface, as indicated (Fig. 1). When the magnetization vector is pointing toward the sample, the intensity of the LCP light is greater than the intensity of the RCP light, whereas the relative magnitude of the two intensities is reversed when the magnetization is pointing away. The overall intensity differences between the two tip orientations are due to the different optical alignments achieved for each separate setup. The degree of circular polarization, $\rho_\gamma = (I_{LCP} - I_{RCP})/(I_{LCP} + I_{RCP})$ corrects for these intensity differences. A value of ρ_γ, averaged over tunneling current and sample bias is also shown (Fig. 1). The sign of the optical polarization changes for the two tip orientations. The photon intensities were also measured with nonferromagnetic W<111> tips (*18*), but $|\rho_\gamma| < 2\%$ and would randomly display both positive and negative values. This small, almost random, polarization may result from the spontaneous electron polarization known to exist in GaAs (*19*). The normalized total luminescence intensity was measured for different tunneling currents and sample biases (Fig. 2). Generally, the total intensity increases as the tunneling current increases in a linear manner (i.e., doubling the tunneling current doubles the light intensity). The total intensity was found to be independent of sample bias, and the error is about the size of the circles. However, for higher currents, the error is larger because of the loss of tunneling stability. The polarization remains unchanged across these data sets (Fig. 1) (*20*).

The pixel-by-pixel topography, tunneling current, total light intensity, and electron polarization acquired with the Ni<110> STM tip with the magnetization vector pointing toward the surface of the sample are shown (Fig. 3). The empty-state STM image (measuring 60 nm by 60 nm) taken with a sample bias of 3.5 V and tunneling current of 12 nA shows two terraces processed with a (110) plane subtraction (Fig. 3A). The dark and light areas represent the terraces separated by a 5.5-nm-high step which has a small kink located near the center of the image. The edge face of the step is in the [$\bar{1}$11] direction and, most likely, is a ($\bar{1}$11) surface. The corresponding pixel-by-pixel tunneling current (Fig. 3B) has a uniform current over the terrace region with an increase (2 nA) over the step region. The data are acquired while the tip is scanning from the lower terrace to the upper terrace (i.e., from upper left to lower right in the images shown in Fig. 3). Scanning over a step typically results in an increase in current due to the delayed response of the feedback circuit pulling the tip away to maintain a constant current. In the corresponding pixel-by-pixel total photon intensity measured from the PMT (Fig. 3C), the most dominant feature is the broad dark strip

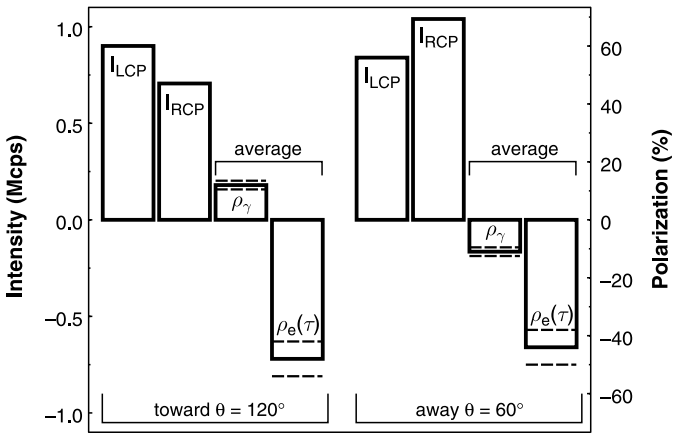

Fig. 1. Intensities of the right (I_{RCP}) and left (I_{LCP}) circularly polarized light, the resulting photon polarization ρ_γ, and the electron spin polarization at the time of recombination $\rho_e(\tau)$, measured for two different orientations of the magnetization vector of the tip. Mcps, million counts per second. The polarizations reported are calculated from multiple intensity measurements using different sample biases and tunneling currents for both tip orientations, with an average value of $|\rho_\gamma| = 11.5 \pm 1.5$. The polarizations remained unchanged for all tested tunneling conditions (2.5 to 3.5 V, 2.5 to 40 nA), even though the intensities did increase for higher tunneling currents (Fig. 2).

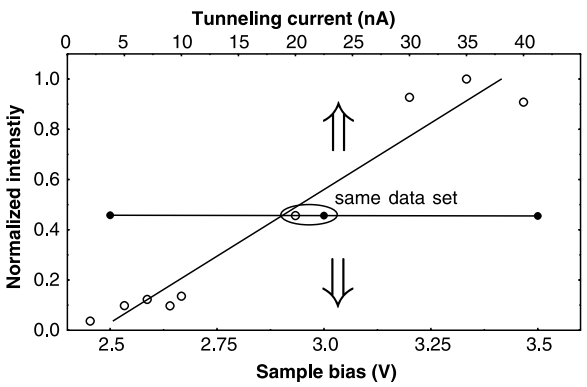

Fig. 2. Total recombination luminescence intensity ($I_{RCP} + I_{LCP}$) versus sample bias and tunneling current. The polarization is constant for all data points (Fig. 1).

that runs vertically through the image, which represents a decrease in the total photon intensity by a factor of ~1000. This decrease occurs despite the increase in tunneling current (Fig. 3B). In the corresponding pixel-by-pixel electron polarization (Fig. 3D), the most dominant feature is the broad bright strip that runs vertically through the image, which represents a change from ~46 to ~8% (from dark to bright, respectively).

Comparison of the intensities and photon polarizations measured over a terrace region and over a step (upper half of Fig. 4) showed that when the tip was tunneling over a step, the intensities of both the LCP and RCP light substantially decreased (by a factor of 500). More important, the polarization of the emitted light also substantially decreased (by a factor of 6).

As indicated earlier, one of the most difficult challenges in making devices that use the spin of the electron is creating a large initial polarization state in the nonferromagnetic semiconductor, denoted here as $\rho_e(0)$ and defined as $(N_\uparrow - N_\downarrow)/(N_\uparrow - N_\downarrow)$, where $N_\uparrow$ and $N_\downarrow$ are the number of up and down spins, respectively. In our experiment, the large measured polarization of the recombination luminescence is indicative of a large initial electron polarization in the GaAs and can be used to calculate its value. For GaAs, because of the spin orbit splitting, ρ_γ depends on the electron spin polarization at the time of recombination, $\rho_e(\tau)$ as follows: $\rho_e(\tau) = 2\rho_\gamma/\cos(\theta)$, where θ is the polar angle between the direction that the electron spin is pointing and the propagation direction of the emitted light that is detected, and τ (2×10^{-10} s^{-1} to 3×10^{-10} s^{-1}) is the recombination lifetime and is independent of temperature, doping species, and doping concentration (*15*, *21*, *22*). These properties of the luminescence are a consequence of the recombination occurring predominantly at the Γ point where the transition is from a simple *s*-wave to *p*-wave type. At this location in *k* space, the light and heavy holes are degenerate and have an equal density, resulting in the factor of 2 in the formula above (*21*, *22*). From this analysis, the average value of $\rho_\gamma(\tau)$ is calculated to be ~46% and is displayed in Fig. 1. The polarization at the time of injection, $\rho_e(0)$, is higher than $\rho_\gamma(\tau)$ because of the bulk spin relaxation processes and can be calculated using

$$\rho_e(0) = \rho_e(\tau)\left(1 + \frac{\tau}{\tau_s}\right) \quad (1)$$

where τ_s (2×10^{-10} s^{-1} to 3×10^{-10} s^{-1}) is the spin relaxation lifetime for p-type GaAs at 100 K (*15*, *21*, *23*, *24*). From Eq. 1, $\rho_e(0)$ is calculated to be ~92% for both tip orientations. In addition, the injection efficiency (IE) of this process is 92%, because the electrons at the Fermi level of the Ni<110> tip are 100% spin polarized (*17*). An alternative interpretation is that the Ni tip is 92% spin polarized and IE = 100%, or some combination in between. Unlike optical methods, which are limited to an initial polarization of 50% by selection rules (*22*), this ballistic method of spin injection can achieve an initial polarization of 100% inside the semiconductor (*25*).

The advantage of using single-crystal Ni<110> tips is that the injection current is nearly 100% spin polarized compared with polycrystalline Ni tips, for which the polarization depends on the crystalline properties of the end of the tip from where the electrons are emitted. With the use of polycrystalline tips, the authors and other groups have achieved initial electron polarizations $\rho_e(0)$ of varying degrees and as high as 48% (*15*). Other simplifications arise when using single-crystal Ni<110> tips: the electron polarization is independent of the tip-to-sample separation, tunneling current, and sample bias because Ni<110> only has one spin at the Fermi level (*15*).

In order to uncover the effect of defects on the spin-relaxation lifetime, the process outlined earlier needs to be performed with nanometer resolution. This is demonstrated by the total intensity drop and polarization change observed in the 10-nm-wide region shown (Fig. 3, C and D). These changes indicate two things: an increase in the number

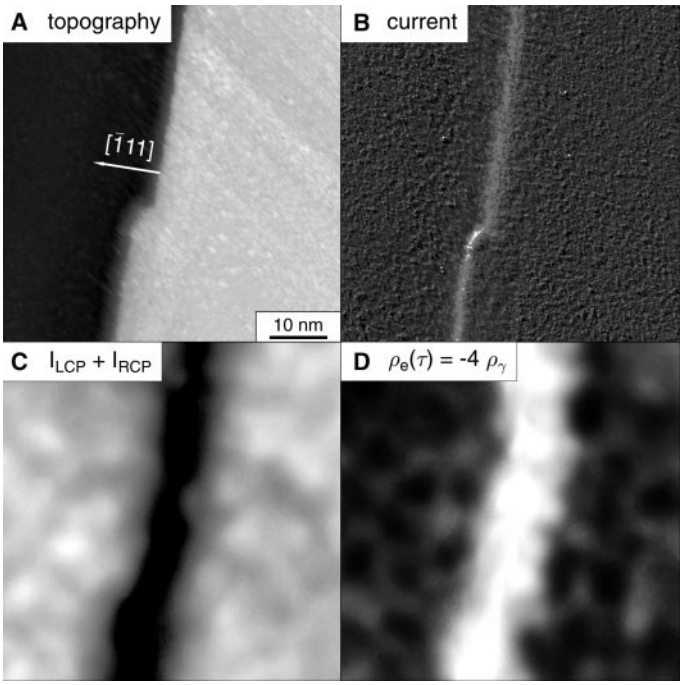

Fig. 3. (**A**) A 60-nm-by-60-nm empty state STM image acquired at 100 K with a sample bias of 3.5 V and a tunneling current of 12 nA. (**B**) Corresponding map of the tunneling current over the same region of surface. (**C**) Corresponding map of the total recombination luminescence intensity. (**D**) Corresponding map of the electron spin polarization.

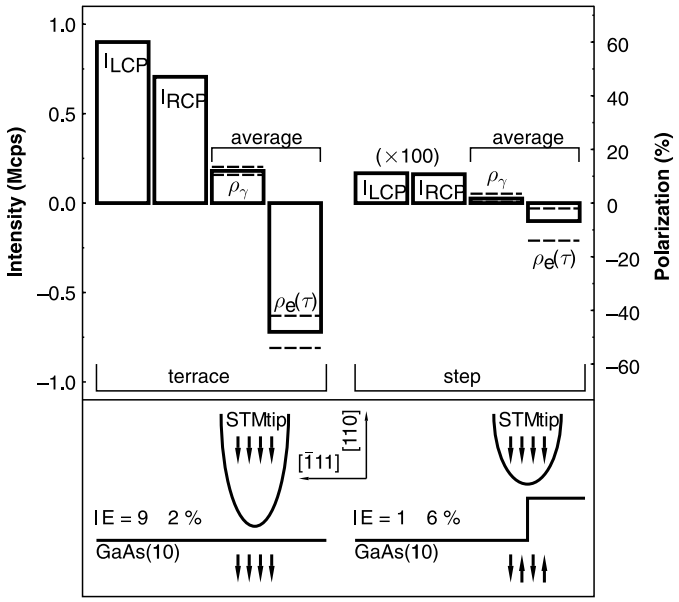

Fig. 4. (**Top**) I_{RCP} and I_{LCP}, ρ_γ, and $\rho_e(\tau)$ measured over a flat terrace and a 5.5-nm-high step. (**Bottom**) Schematic of the tip over a flat surface and step (with crystallographic direction arrows) and its effect on the IE.

of nonradiative recombination paths and a change in the spin-injection probability. Acquiring this polarized photon intensity map of the surface required a current source with a large degree of polarization, a sample temperature of 100 K, and good collection optics to obtain a large enough photon signal to sample in tandem with the STM topography. With the use of the calculational method discussed earlier, the optical polarization measured at the step edge can be used to find the initial electron polarization. The electron polarization at the time of recombination is found to be ~8% (Fig. 4, upper half). From Eq. 1, the initial electron polarization is calculated to be ~16%. This corresponds to an IE of only 16% (Fig. 4, lower half). The dramatic decrease (by a factor of 6) in injection efficiency indicates that the step edge causes a substantial amount of spin-flip scattering. If we assume that the initial polarization state over the step is 100%, then we can calculate a local spin-relaxation lifetime by solving Eq. 1 for τ_s and relabeling it as τ_s^{step}

$$\tau_s^{step} = \tau\left[\frac{\rho_e(0)}{\rho_e(\tau)} - 1\right] \qquad (2)$$

After substitution, $\tau_s^{step} \approx \tau/12$, and in terms of the bulk spin-relaxation lifetime, $\tau_s^{step} \approx \tau_s/12$. This means that the step scatters spins 12 times faster than the bulk processes.

Little is known about why a particular defect, such as a step edge, disrupts the spin injection process. Previous findings show that midgap states decrease the carrier lifetime (*26*), which suggests that midgap states may play an important role in decreasing the spin-relaxation lifetime (*27*). In our situation, we have the ability to compare the spin-injection properties of the GaAs(110) terrace with a [$\bar{1}$11]-oriented step. The electronic properties of these two features are very different in an important and revealing way. First, the GaAs(110) terrace has no midgap states, making it appear electronically similar to bulk GaAs, so one might expect to obtain the bulk spin relaxation lifetime when injecting over a flat GaAs(110) terrace (*28*). Second, the [$\bar{1}$11]-oriented step is most likely a GaAs(111) surface, which does have midgap states; in fact, it is found to be metallic (*29*). This metallic property has two profound implications for understanding our results. Firstly, this indicates that there would be nonradiative, phonon channels to the valence band states, explaining the large decrease in light intensity. Secondly, the half-filled bonds would create unpaired spins which could substantially affect the spin-injection process through spin-spin scattering events, explaining the reduction in the spin-relaxation lifetime when injecting over the step. From this analysis the height of the step does play an important role, because higher steps would have a larger number of metallic-like bonds than shorter steps, thereby increasing the likelihood of spin- flip scattering events (*30*).

References and Notes

1. S. Datta, B. Das, *Appl. Phys. Lett.* **56**, 665 (1990).
2. G. A. Prinz, *Phys. Today* **48** (no. 4), 58 (1995).
3. D. D. Awschalom, J. M. Kikkawa, *Phys. Today* **52** (no. 6), 33 (1999).
4. H. Ohno, *Science* **281**, 951 (1998).
5. H. Ohno *et al.*, *Appl. Phys. Lett.* **69**, 363 (1996).
6. J. M. Kikkawa, D. D. Awschalom, *Nature* **397**, 139 (1999).
7. P. R. Hammar, B. R. Bennett, M. J. Yang, M. Johnson, *Phys. Rev. Lett.* **83**, 203 (1999).
8. S. Gardelis, C. G. Smith, C. H. W. Barnes, E. H. Linfield, D. A. Ritchie, *Phys. Rev. B* **60**, 7764 (1999).
9. R. Fiederling *et al.*, *Nature* **402**, 787 (1999).
10. Y. Ohno *et al.*, *Nature* **402**, 790 (1999).
11. B. T. Jonker *et al.*, *Phys. Rev. B* **62**, 8180 (2000).
12. R. Wiesendanger, *Scanning Probe Microscopy and Spectroscopy, Methods and Applications* (Cambridge Univ. Press, Cambridge, 1994).
13. R. Berndt *et al.*, *Phys. Rev. Lett.* **74**, 102 (1995).
14. P. Renaud, S. F. Alvarado, *Phys. Rev. B* **44**, 6340 (1991).
15. S. F. Alvarado, P. Renaud, *Phys. Rev. Lett.* **68**, 1387 (1992).
16. S. F. Alvarado, *Phys. Rev. Lett.* **75**, 513 (1995).
17. E. Kisker, W. Gudat, E. Kuhlmann, R. Clauberg, M. Campagna, *Phys. Rev. Lett.* **45**, 2053 (1980).
18. The tips were electrochemically etched under high magnification (×500) with a 10% HCl solution and then loaded into a UHV chamber (4 $\times 10^{-11}$ to 8 $\times 10^{-11}$ torr) that contains a commercially available variable-temperature STM. To remove any native oxide, the tips were then cleaned in situ with electron-beam heating and placed on the STM imaging stage, with the magnetization directed either away from or toward the surface of the sample. For control purposes, nonmagnetic single-crystal <111>-oriented W tips were also used. These were etched with NaOH but were otherwise prepared in the same manner as the Ni tips. The GaAs(110) surfaces were prepared by cleaving p-type GaAs(001) wafers [Zn doped, hole density (p) = 1.25 × 10^{19} cm^{-3}, carrier mobility (μ) = 100 cm^2/volt seconds (Vs), x-ray (004) linewidth <10 arc sec, and etch pit density <3000/cm^2 over 100% of the area] in situ, which produces a clean, nearly atomically flat cross-sectional (110) surface. The samples were then placed on the STM stage and cooled with a cold finger immersed in liquid nitrogen. The temperature of the STM stage was measured to be 77 K, and we estimate the sample temperature to be ≈ 100 K, whereas the STM tip is not cooled and is assumed to be at room temperature.
19. S. F. Alvarado, H. Riechert, N. E. Christensen, *Phys. Rev. Lett.* **55**, 2716 (1985).
20. B. Fromme, G. Baum, D. Gockel, W. Raith, *Phys. Rev. B* **40**, 12312 (1989).
21. G. E. Pikus, A. N. Titkov, in *Optical Orientation*, F. Meier, B. P. Zakharchenya, Eds. (Elsevier, New York, 1984), pp. 73–131.
22. D. T. Pierce, F. Meier, *Phys. Rev. B* **13**, 5484 (1976).
23. R. C. Miller, D. A. Kleinman, W. A. Nordland Jr., R. A. Logan, *Phys. Rev. B* **23**, 4399 (1981).
24. K. Zerrouati *et al.*, *Phys. Rev. B* **37**, 1334 (1988).
25. G. Schmidt, D. Ferrand, L. W. Molenkamp, A. T. Filip, B. J. van Wees, *Phys. Rev. B* **62**, R4790 (2000).
26. B. T. Jonker, O. J. Glembocki, R. T. Holm, R. J. Wagner, *Phys. Rev. Lett.* **79**, 4886 (1997).
27. M. W. J. Prins *et al.*, *J. Phys. Condens. Matter* **7**, 9447 (1995).
28. R. M. Feenstra, J. A. Stroscio, J. Tersoff, A. P. Fein, *Phys. Rev. Lett.* **58**, 1192 (1987).
29. D. K. Biegelsen, R. D. Bringans, J. E. Northrup, L. E. Swartz, *Phys. Rev. Lett.* **65**, 452 (1990).

30. We thank M. Klotz and S. Singh for their helpful comments. Supported by the Office of Naval Research (grant N00014-97-1-1058), NSF (grants DMR-9733994, DMR-0080054, and DMR-0102755), and Research Corporation (grant RI0153).

30 January 2001; accepted 11 April 2001

MgB_2 Superconducting Thin Films with a Transition Temperature of 39 Kelvin

W. N. Kang,* Hyeong-Jin Kim, Eun-Mi Choi, C. U. Jung, Sung-Ik Lee

We fabricated high-quality *c* axis–oriented epitaxial MgB_2 thin films using a pulsed laser deposition technique. The thin films grown on (1 $\bar{1}$ 0 2) Al_2O_3 substrates have a transition temperature of 39 kelvin. The critical current density in zero field is ~6 × 10^6 amperes per cubic centimeter at 5 kelvin and ~3 × 10^5 amperes per cubic centimeter at 35 kelvin, which suggests that this compound has potential for electronic device applications, such as microwave devices and superconducting quantum interference devices. For the films deposited on Al_2O_3, x-ray diffraction patterns indicate a highly *c* axis–oriented crystal structure perpendicular to the substrate surface.

The recent discovery of the binary metallic MgB_2 superconductor (*1*) having a remarkably high transition temperature (T_c) of 39 K has attracted great scientific interest (*2–8*). With its metallic charge carrier density (*2*) and the strongly linked nature of its intergrains in a polycrystalline form (*9*, *10*), this material is a promising candidate for superconducting devices (*11*) as well as large-scale applications. Furthermore, because single-crystal growth of MgB_2 seems very difficult, the fabrication of epitaxial thin films should be an important development for future basic research studies.

National Creative Research Initiative Center for Superconductivity, Department of Physics, Pohang University of Science and Technology, Pohang 790–784, Korea.

*To whom correspondence should be addressed. E-mail: wnkang@postech.ac.kr